Title	Highly Ordered Mesoporous Hydroxide Thin Films through Self-Assembly of Size-Tailored Nano-Building Blocks: A Theoretical- Experimental Approach
Author(s)	Tarutani, Naoki; Tokudome, Yasuaki; Jobbágy, Matías; Soler-Illia, Galo J. A. A.; Tang, Qiyun; Müller, Marcus; Takahashi, Masahide
Citation	Chemistry of Materials , 31 (2) : 322 - 330
Issue Date	2018-12-27
DOI	10.1021/acs.chemmater.8b03082
Self DOI	
URL	https://ir.lib.hiroshima-u.ac.jp/00053532
Right	© 2018 American Chemical Society This document is the Accepted Manuscript version of a Published Work that appeared in final form in Chemistry of Materials, copyright © American Chemical Society after peer review and technical editing by the publisher. To access the final edited and published work see https://doi.org/10.1021/acs.chemmater.8b03082 This is not the published version. Please cite only the published version. この論文は出版社版ではありません。引用の際には出版社版をご確認、ご利用ください。
Relation	


Hiroshima University Institutional Repository

Highly Ordered Mesoporous Hydroxide Thin Films through Self-Assembly of Size-Tailored Nano-Building Blocks: A Theoretical-Experimental Approach

Naoki Tarutani[†], Yasuaki Tokudome*[†], Matías Jobbágy[§], Galo J. A. A. Soler-Illia*[#], Qiyun Tang[‡], Marcus Müller[‡], Masahide Takahashi[†].

[†]Department of Materials Science, Graduate School of Engineering, Osaka Prefecture University, Sakai, Osaka 599-8531, Japan

[§] INQUIMAE-CONICET, Facultad Ciencias Exactas y Naturales, Universidad de Buenos Aires, Buenos Aires, C1428EHA, Argentina

[#] Instituto de Nanosistemas, Universidad Nacional de General San Martín, Av. 25 de Mayo y Francia, San Martín, 1650, Argentina

[‡] Institut für Theoretische Physik, Universität Göttingen, Friedrich-Hund-Platz 1, 37077 Göttingen, Germany

KEYWORD: Crystalline mesoporous materials, assembly of nano-building block approach, layered hydroxides, epoxide-mediated alkalinization, coarse-grain simulation

ABSTRACT: Mesoporous crystalline (hydr)oxides of low-valence metal ions (M(II) and M(III)) are highly demanded in the context of various applications. In this study, we demonstrate key factors to the successful formation of ordered mesoporous films through the Assembly of Nano-Building Block (ANBB) approach using a colloidal solution of crystalline $M(OH)_2$ (M = Mn, Fe, Co, Ni, and Cu). The colloidal system of α-$Ni(OH)_2$ is presented in-depth as a typical example. Crystal growth and aggregation kinetics of the NBB were tuned by synthetic parameters. Nanometer-sized NBBs of tailored size between oligomer scale to over 20 nm were obtained. The films prepared from α-$Ni(OH)_2$ NBBs with a diameter of ≤ 7.5 nm showed ordered mesostructures through evaporation-induced self-assembly in the presence of supramolecular templates. Coarse-grained simulation suggests that there is a threshold diameter of NBB toward the formation of well-ordered mesostructures. It was found that, as well as limiting the diameter of NBB, inhibition of an aggregation of NBBs by using coordinative additives or diluting the NBB colloidal solution were essential to control the assembly of NBBs and templates into the ordered mesostructures. The results obtained here open up the synthesis of ordered mesoporous materials with a crystalline wall of variety of chemical compositions containing low-valence metal elements.

Introduction

The bottom-up synthesis of mesoscale architectures from pre-formed nano-building blocks (NBBs) is a promising way to design functional materials. In the last few years, superstructures constituted of nanocrystals,[1] anisotropic oriented structures,[2] porous systems,[3] gradient periodic structures[4] and co-continuous structures[5] fabricated through the NBB approach have been reported. These architectures show advantageous characteristics in wide application fields such as catalysts,[6] optical materials,[7] and energy storage.[8] The chemical composition and the crystalline phase of these materials can be tuned by tailoring the respective NBBs. Moreover, specific interfaces and heterostructures can be formed by the use of NBBs with different chemical and structural features. Intrinsic properties of NBBs are then combined, and a synergic effect leads to novel functionalities.[9,10]

In the case of mesoporous materials, a precise tuning of the NBB diameter, D_{NBB}, and their assembly process are highly demanded. The desired architectural features are regulated by the D_{NBB} and interaction of organic and inorganic NBBs .[11] The Assembly of NBBs (ANBB) approach has been employed for the fabrication of ordered mesoporous materials with enhanced liquid/ion diffusion, high specific surface area, and alignment of the pores. However, the preparation of single-nm-sized "crystalline" NBBs and their assembly into ordered mesostructures are so far limited to high-valence metal oxides such as ZrO_2, TiO_2, and CeO_2. [12-14] Technologically valuable crystalline (hydr)oxides of low-valence metal elements (M(II) and M(III)) rapidly form coarse μm-sized crystals and aggregates, which prevents assembly into ordered mesostructures. These materials are highly desirable in electrochemical catalysts, sustainable energy devices, and environmental treatment.[15-18]

Recently, we reported the preparation of single-nm-sized low-valence metal hydroxide nanocrystals with a variety of chemical compositions.[19] The nanocrystals were obtained as colloidal solutions and could be used as inorganic NBBs to form well-defined mesoporous structures via an evaporation-induced self-assembly (EISA) process. Mesoporous films made of $Ni(OH)_2$ NBBs exhibit pseudocapacitance of 169 times as high as their non-mesoporous counterparts. While this breakthrough permitted to access several (hydr)oxide frameworks, the effect of diameter and stability of the metal hydroxide NBBs, which in turn depends on a chemical composition of NBBs, on the final mesoporous structures are only incompletely understood. The formation of ordered mesoporous structures is still limited to NBBs of particular compositions.

Herein, we demonstrate key factors towards the compositionally versatile formation of crystalline ordered mesoporous films from metal hydroxide NBBs. The diameter and the aggregative kinetic of NBBs were tuned by synthetic parameters of the epoxide-mediated alkalinization process, and their effects on the final mesoporous structures were systematically investigated. We successfully controlled the diameter of NBBs, D_{NBB}, from the oligomeric scale to over 20 nm by tuning the amount of additives and reaction time. Ordered mesoporous films were found to form through an EISA process for D_{NBB} smaller than a threshold value. Simulation studies showed a good agreement with experimental, indicating that there is a threshold of D_{NBB} toward the formation of well-ordered mesostructures. It was found that the aggregation tendency of NBBs is another important factor for the formation of well-defined mesostructures. The crystallization and aggregation of NBBs strongly depend on the chemical composition of the starting solutions. The present tunable synthesis route of NBBs with a variety of compositions gives us general insights about NBBs for the successful formation of ordered mesostructures (hydroxide of Mn, Fe, Co, Ni, and Cu). Moreover, the mesoporous metal hydroxide films produced through this route can be transformed into oxides, sulfide, and carbon/metal composites by post-treatment. The present synthesis is therefore promising to improve the functional properties of diverse mesoporous materials.

Experimental

Chemicals.

Manganese(II) chloride tetrahydrate ($MnCl_2 \cdot 4H_2O$, 99.0%), iron(II) chloride tetrahydrate ($FeCl_2 \cdot 4H_2O$, 99.0-102.0%), cobalt chloride hexahydrate ($CoCl_2 \cdot 6H_2O$, 99.0%), nickel chloride hexahydrate ($NiCl_2 \cdot 6H_2O$, 98.0%), copper chloride dihydrate ($CuCl_2 \cdot 2H_2O$, 99.0%) acetic acid (99.7%), acrylic acid (99%), glutaric acid (98.0%), citric acid (98.0%), ethanol (99.5%), (±) propylene oxide (> 99%), and Pluronic F127 (poly(ethylene oxide)-poly(propylene oxide)-poly(ethylene oxide), PEO-PPO-PEO) were used as received. Acrylic acid, propylene oxide and F127 were purchased from Sigma-Aldrich Co. All other reagents were purchased from Wako Pure Chemicals Industries, Ltd. Ultrapure water of 18.2 MΩ·cm resistivity was used in all experiments.

Synthesis of α-$Ni(OH)_2$ NBBs.

$NiCl_2 \cdot 6H_2O$ (0.5 mmol) and a given amount of carboxylic acid (acrylic acid or acetic acid) (molar ratio of carboxylic acid to nickel chloride was 0–4.0) were dissolved in an ethanol (1.0 mL) at 25 °C. Propylene oxide (7.5 mmol) was added to the clear precursor solution and stirred for 30 s. Resultant homogenous solutions were left at room temperature (20–25 °C). Variety of in-situ measurements were taken during reaction progress. After an appropriate time, the samples were dried at 60 °C for 20 h. The sample IDs prepared through this process are denoted as *x*-*y*-*t*, where *x* is the type of acid (AA; acrylic acid and AcOH; acetic acid), *y* is the molar ratio of carboxylic acid to nickel chloride, and *t* is the time (min) since the addition of propylene oxide.

Synthesis of mesoporous α-$Ni(OH)_2$ cast-films.

$NiCl_2 \cdot 6H_2O$ (0.5 mmol), carboxylic acid (acrylic acid or acetic acid) (0–4.0 mmol) and template surfactant (F127) (32 mg, $[F127]/[Ni^{2+}]=0.005$) were dissolved in ethanol (1.0 mL) at 20–25 °C. After the addition of propylene oxide (7.5 mmol), the solution was stirred for 30 s and left at 20–25 °C. The reacting solution was casted on glass (76 mm × 26 mm) or Si substrates (~ 20 mm square) after an appropriate time and allowed to evaporate under ambient conditions (temperature; 20–25 °C, humidity; 50–70 %) for 2 h. As-synthesized films were left in an oven at 60 °C for 2 h, followed by a treatment at 120 °C for 2 h. To remove polymer templates, films were heat treated at 250 °C for 2 h. The sample IDs are denoted as F-*x*-*y*-*t*, where *x*, *y*, and *t* are same as described above.

Synthesis of mesoporous $M(OH)_2$ (M = Mn(II), Fe(II), Co(II), Ni(II) and Cu(II)) cast-films.

$MCl_2 \cdot nH_2O$ (M = Mn(II), Fe(II), Co(II), Ni(II) and Cu(II), *n* = 2–6) (0.5 mmol), carboxylic acid (acrylic acid (4.0 mmol), glutaric acid (1.0 mmol), or citric acid (0.67 mmol)) and F127 (32 mg) were dissolved in an ethanol (1.0 mL) at 20–25 °C. After the addition of propylene oxide (7.5 mmol), the solution was stirred for 30 s and left at 20–25 °C. The reacting solution was casted on glass substrate after an appropriate time, and then allowed to evaporate under an ambient condition (temperature; 20–25 °C, humidity; 50–70 %) for 2 h. The sample IDs are denoted as *M*-*x*-*y*-*t*, where *M* is metal ion (Mn, Fe, Co, Ni and Cu), *x* is kind of carboxylic acid (AA: acrylic acid, Glu: glutaric acid, and Cit: citric acid), *y* and *t* are same as described above, respectively.

Simulation studies.

A coarse-grained model of α-$Ni(OH)_2$ NBBs and amphiphilic surfactant, F127, was employed to study the formation of mesostructures. The α-$Ni(OH)_2$ NBBs were represented by spherical nanoparticles with variable diameters, and the surfactant F127 was described by a soft bead-spring model of a BAB triblock copolymer (PEO-PPO-PEO). The effect of solvents such as water and acid are taken into account in the interactions between NBBs

and surfactants.[20] The Hamaker potential was chosen for NBB-NBB interaction, in which the magnitude of the potential depends on the D_{NBB}. Details of the model are summarized in the supporting information.

The dispersity index (DI) was calculated to evaluate the homogeneity of mesostructures. The DI is defined as DI = S_w/S_n, where $S_w = \Sigma_i n_i \sigma_i^2 / \Sigma_i n_i \sigma_i$ is the weight average pore area and $S_n = \Sigma_i n_i \sigma_i / \Sigma_i n_i$ is the number average pore area. Here n_i is the number of mesopores with area, σ_i, obtained from 10 independent simulations; in each simulation 100 configurations are selected for the DI calculation.

Characterization.

A transmission electron microscope (TEM; JEM-2000FX, JEOL, Japan) and scanning TEM (STEM; JEM-2100F, JEOL, Japan) were employed at an operating voltage of 200 kV to observe primary particles and mesostructures of the samples. Powder X-ray diffraction (PXRD) (Multiflex, Rigaku, Japan) using Cu Kα radiation (λ = 0.1544 nm) was used to characterize crystal phases of dried powdery samples. Fourier transform infrared (FT-IR) spectroscopy (ALPHA FT-IR spectrometer, Bruker Optik GmbH, Germany) and ultraviolet-visible-near infrared (UV-Vis-NIR) spectroscopy (V-670 spectrophotometer, JASCO Corp.) were used to analyze chemical bonding and coordination state of Ni(II). Conductivity and pH of solutions were collected using a water quality meter (D74, Horiba, Japan) with respective glass electrodes (3552-10D and 9618-10D). The mesoporous characteristics of samples heat-treated at 250 °C were analyzed by N_2 sorption measurements (Belsorp-mini II, Bel Japan Inc., Japan). Small angle X-ray scattering (SAXS) measurement was performed to characterize the D_{NBB} and mesostructures with the beamline of the Brazilian Synchrotron Light Laboratory (LNLS, Brazil D11A-SAXS1-18927 and 20160366). A polyimide film was used to pack and measure the powder samples. The D_{NBB} is defined as the diameter of aggregates when primary particles form aggregation. Details of characterization are described in Supporting Information.

Results and discussion

Synthesis of α-Ni(OH)$_2$ NBBs of controlled diameter.

Uniform colloidal dispersions of nickel hydroxides with particle diameters ranging from 2 to 20 nm were obtained after aging the metal chloride in the presence of propylene oxide and an organic acid at room temperature. Hydrolysis of propylene oxide increases the solution pH homogeneously,[21] inducing a high degree of supersaturation to form nm-sized hydroxide crystals,[22] while the organic acid controls the growth kinetics of the metal hydroxide. Figure 1a shows a typical sample obtained from the reaction mixture containing $NiCl_2 \cdot 6H_2O$ and acrylic acid (AA-2.0-60). The powder obtained by drying the colloidal dispersion can be identified as nanometer sized α-Ni(OH)$_2$ which grow preferentially along the *c* axis (Figure 1b). Acrylic acid was mandatory to yield a stable colloidal solution. Indeed, opaque gelatinous products due to high aggregation of the inorganic building blocks were obtained from a reaction mixture without acrylic acid (Figure S2). This result suggests that the addition of acrylic acid is a key factor to control the crystal growth and to inhibit the aggregation of nanocrystals.

One desirable feature of this synthetic pathway is the possibility of an accurate kinetic and thermodynamic control of D_{NBB} through external synthetic variables such as initial concentrations, amount of propylene oxide, type of acid employed, or reaction time.

This approach is illustrated by analyzing in-depth a reactive system that uses acrylic acid as a growth controller. Figure 2a shows the evolution of D_{NBB} as a function of the reaction time for an exemplary system, AA-2.0-*t* systems, which evolves for *t* = 1–60 min. D_{NBB} were estimated from the in-situ SAXS patterns collected for the reacting medium (see Supporting information for the details). A linear increase of the D_{NBB} is observed, from the oligomer scale to ~ 1.5 nm in the first 15 minutes. The growth levels off in a second step, and the final diameter is almost reached in the first 30 min, which is in a good agreement with the time scale of the consumption of ionic species. The relative amount of Ni(II) ion decreases to 6.1% of the initial concentration within 30 min reaction. The crystal growth of layered nickel hydroxide was reported to take place through rapid edge-on condensation of partially hydrolyzed Ni species, followed by a relatively slow stacking of the sheets.[23] In the present case, the extended growth of the constituent sheets was successfully retarded by the addition of acrylic acid. FT-IR, UV-Vis-NIR, and PXRD measurements revealed that most changes due to nanocrystal growth take place in the first 30 minutes of reaction (Figure S3). Racah B parameter and crystal field energy of AA-2.0-*t* were estimated from UV-Vis-NIR spectra and reached constant values comparable with reported α-Ni(OH)$_2$ (Figure S3b and S3d),[24,25] which means brucite-like hydroxide sheets were successfully formed. FT-IR signals belonging to the asymmetric $\nu(COO)_{as}$ and symmetric $\nu(COO)_s$ acrylate vibrations were observed in the 1582–1552 cm^{-1}, and 1428 cm^{-1} regions, respectively (Figure S3a). The frequency differences $\Delta = \nu(COO)_{as} - \nu(COO)_s$, were in the range of 124–154 cm^{-1}, which is relatively larger or comparable to that of free acrylate (Δ = 110–140 cm^{-1}).[26] These results suggest acrylate ion is unidentately coordinated to Ni(II) and intercalated/adsorbed on α-Ni(OH)$_2$ sheets.[25] It can be concluded that acrylic acid is present in the NBB through unidentate coordination to a small number of Ni(II) centers, and intercalation.

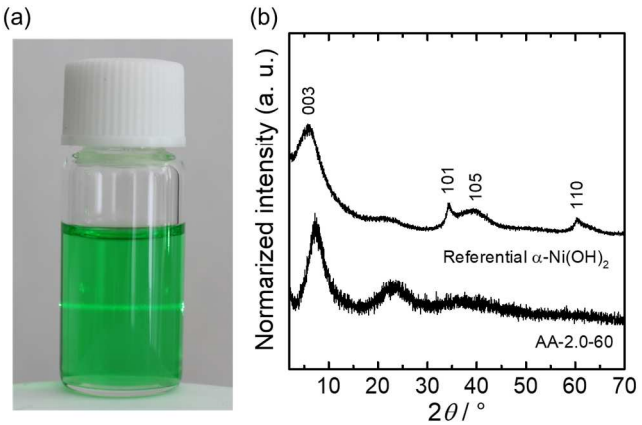

Figure 1. (a) Transparent solution of AA-2.0-60 showing Tyndall effect. (b) PXRD pattern of powder collected by drying AA-2.0-60 solution. The referential pattern was acrylate intercalated α-Ni(OH)$_2$ prepared by a standard precipitation method (see Supporting information).

Individual nanocrystals remain well dispersed in the initial solutions when AA/Ni > 2.0. The STEM image of synthesized NBB (Figure 2b) shows that the D_{NBB} was 1.8 nm without aggregation, which supports the result of SAXS measurement. The diameter of NBB obtained under these synthetic conditions is relatively small compared to previously reported oxide systems (~ 5 nm),[12-14] which should allow the flexible tuning of the mesostructure through controlled interactions among organic and inorganic NBBs.

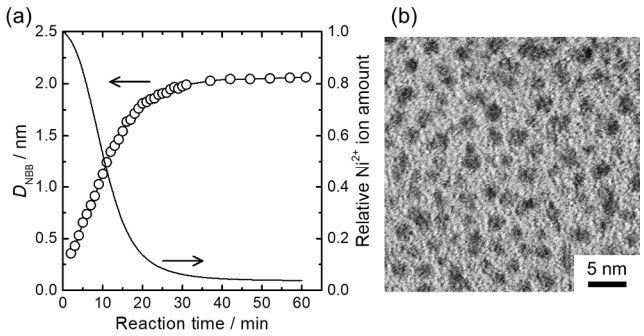

Figure 2 Time evolution of D_{NBB} (open circle) and consumption of ionic Ni species (solid line) (calculated from conductivity of solution, see ESI) in the reacting solution of AA-2.0-*t* (*t* = 1–60 min). (b) STEM image of AA-2.0-60 dried on a TEM copper grid.

TEM observations indicated that samples obtained from solutions with lower amount of acrylic acid (AA/Ni < 2.0) were composed of aggregated fine nanoparticles (shown in the Experimental Section of ESI). Therefore, a hierarchically structured model was employed for fitting the SAXS curves of reactive systems containing lower amount of organic acids, i.e., AA-*y*-*t* (*y* = 0–1.0, *t* = 1–60 min), in order to take into account the aggregation of the NBBs. Time-evolution of primary and secondary particle diameters are presented in Figure 3a. All solutions contained secondary particles after an appropriate reaction time. The nanoparticle growth rates were estimated by linear fitting of the obtained plot. The primary particles grew at a rate of 0.37 nm/min (AA-0-*t*), 0.25 nm/min (AA-0.1-*t*), 0.33 nm/min (AA-0.5-*t*) within the first 10 min, and the diameter of the primary particles, D_p, reached a value of ~ 2.0 nm irrespective of the amount of acrylic acid. On the other hand, the growth rates of the secondary particles, D_s, were retarded by increasing amounts of acrylic acid (AA-0-*t*; 7.5 nm/min, AA-0.1-*t*; 2.9 nm/min, AA-0.5-*t*; 0.61 nm/min). Figure 3b shows D_{NBB} prepared with various amounts of acrylic acid after 30 min reaction (D_p or D_s were used as D_{NBB} for the system without or with aggregation, respectively). It is clearly observed that D_{NBB} decreased from > 20 nm (aggregated particles) to ~ 2 nm (isolated particles) with increasing amounts of acrylic acid. These results indicate that acrylic acid not only retards the crystallization but also suppresses the aggregative tendency of NBBs, through coordination, intercalation, and surface modification. In summary, D_{NBB} were successfully controlled from oligomer scale to > 20 nm by tuning the reaction time and the amount of acrylic acid. This procedure permits to tailor the size and interactions between the inorganic NBBs, in order to create hybrid meso-architectures. It is important to stress that after reaction completion (i.e., removal of Ni(II) from solution), no significant changes are observed in D_{NBB} for several days, so it can be reasonably concluded that after a first kinetic evolution, the control of D_{NBB} is attainable in a practically thermodynamic fashion.

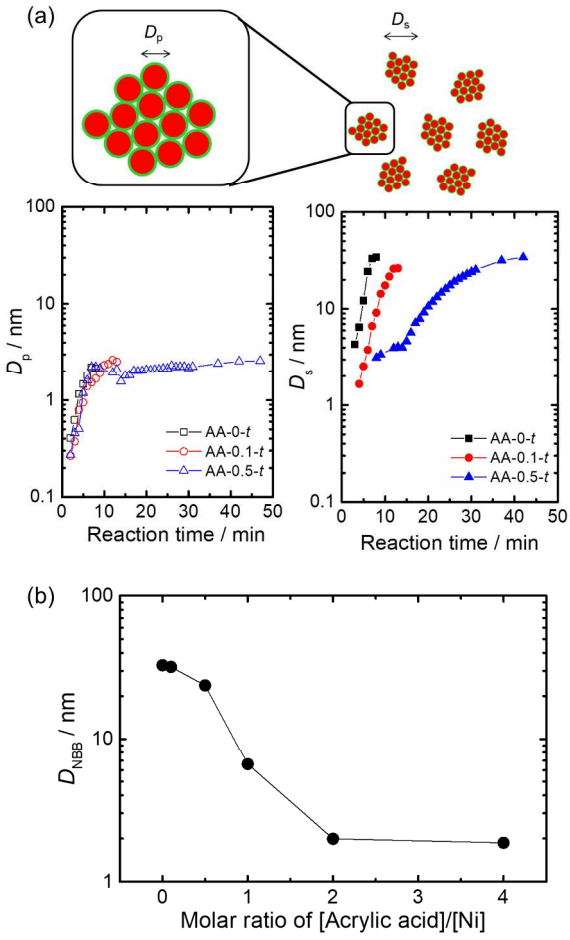

Figure 3. (a) Time-dependent growth of the diameters of primary particles, D_p (open symbols), and secondary particles, D_s (close symbols), prepared from AA-0-*t* (black), AA-0.1-*t* (red), and AA-0.5-*t* (blue) (*t* = 1–60). (b) Molar ratio ([AA]/[Ni]) dependence of D_{NBB} (D_s when AA/Ni ≤ 1.0 and D_p when AA/Ni ≥ 2.0) of AA-*y*-30 (*y* = 0–4.0).

The effect of D_{NBB} on the formation of mesoporous structures

The α-$Ni(OH)_2$ NBBs with different diameters could be tunably produced and were used to elucidate dominant factors towards the successful formation of mesoporous crystalline films. A nonionic block-copolymer, F127, was used as the supramolecular pore template. The addition of F127 to the initial solutions had little effect on the growth and aggregation of NBBs (Figure S4). While this fact permitted us to keep design D_{NBB}, the controlled drying of cast sols containing also the template allowed for the co-self-assembly of NBBs and F127 templates.

Solutions containing NBBs of varying diameter D_{NBB} from 0.74 to 26 nm were employed to fabricate mesostructured films through the EISA process, in a systematic experiment (Figure 4a). The cast-film prepared by using NBBs of D_{NBB} ≤ 7.5 nm showed SAXS peaks assigned to an organized mesostructure. TEM micrographs and the N_2 adsorption isotherm showed cubic-like patterns (Figure 4b and S5), which could then be confirmed by indexation as derived from an *Im–3m* structure formed by inorganic NBB located around initially spherical micelles. The obtained ordered 3D cubic mesostructure was maintained even after removal of F127 template by heat treatment at 250 °C. The threshold of D_{NBB} toward the ordered mesostructure formation, 7.5 nm, demonstrated in this study is valid for previously reported mesoporous metal oxides with F127 templates, where the sizes of NBBs are smaller than a critical size for all the successful examples, which is linked to a size of building block that permits to flexibly adapt to the micelle curvature.[14,26]

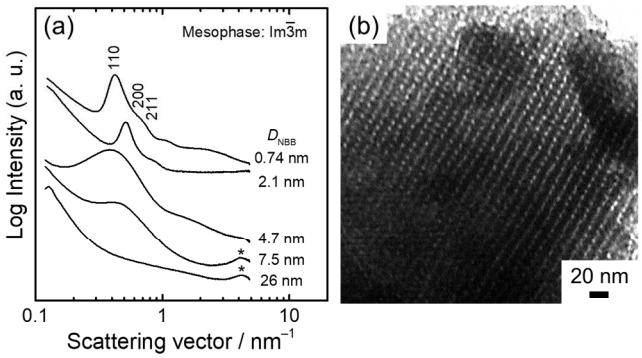

Figure 4. (a) SAXS patterns of cast-films after drying at 120 °C for 2h. The casted-films composed of D_{NBB} = 0.74 nm, 2.1 nm, 4.7 nm, 7.5 nm, and 26 nm were prepared from F-AA-2.0-5, F-AA-2.0-60, F-AA-0.5-15, F-AA-1.0-45, and F-AA-0.1-15, respectively. *: background peaks from α-$Ni(OH)_2$ and polyimide. (b) TEM image of films prepared from AA-2.0-F-5 after heat treatment at 120 °C for 2 h and 250 °C for 2 h.

The samples prepared with NBB of 4.7 nm ≤ D_{NBB} ≤ 7.5 nm showed a broad peak at q ~ 0.5 nm^{-1}. The broadening of the peak for these samples reveals that the mesostructure becomes less-ordered when larger inorganic NBB are used as precursors.

In order to understand the role of the NBB in the formation of organized mesostructures, we performed a simulation study that takes into account the size and interactions of the inorganic NBB and the templates. The model considers n amphiphilic surfactants and n_P nanoparticles in the canonical ensemble. The inorganic NBBs are modelled as spherical NPs, which interact which each other via a Hamaker potential.[27] The PEO-based surfactant, F127, is represented by a bead-spring model with soft, non-bonded interactions,[28] and the molecule is discretized into N = 40 coarse-grained beads with a structure of $B_{14}A_{12}B_{14}$. The end-to-end distance of F127 can be calculated as $R_{eo} \approx \sqrt{6}R_g$ = 8.475 nm, where R_g = 3.46nm is the radius of gyration for F127, measured from SAXS experiments. This top-down model incorporates bonded interactions that describe the linear chain architecture and non-bonded interactions that give rise to microphase separation in the surfactant solution.[20] Details of the calculation and potentials used are provided in the ESI.

Figures 5a and 5b show snapshots from the simulation system with the extreme values of D_{NBB} = 2.54 and 5.94 nm, respectively, after the system has reached a stationary state. While in the first case a very well-ordered mesostructure is observed, the system with larger NBB size shows significantly less-ordered mesostructures (see Figure S6 and further discussion in supplementary information). To evaluate the homogeneity of the mesostructure, the dispersity index (DI) was calculated for each simulation system (Figure 5c). DI is a criterion of a homogeneity of mesostructure in this study, a smaller DI signals implies a more homogenous mesostructure. While a relatively constant value of DI is observed for low NBB diameters, which is indicative of a well-defined mesostructure, a rapid increase of DI is observed between D_{NBB} = 4.24 and 5.08 nm. This result indicates that the mesostructures becomes less ordered when D_{NBB} grows beyond a critical value.

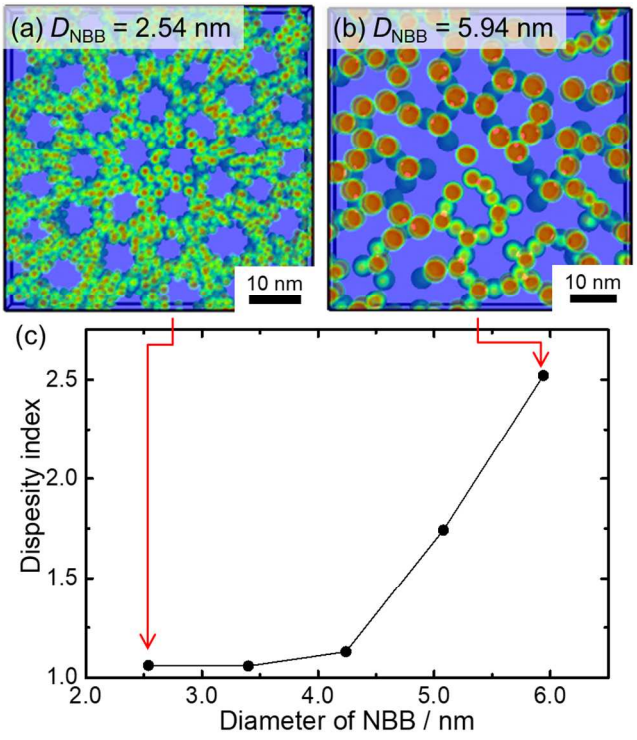

Figure 5. Typical snapshots of mesostructures formed with NBBs and F127 with D_{NBB} = (a) 2.54 nm and (b) 5.94 nm. The system size of (a) is 61.02 × 61.02 × 7.63 nm^3 and of (b) is 68.65 × 68.65 × 7.63 nm^3. The red spheres, green rings and blue regions are the NBB core, the interface and the F127 filled parts, respectively. (c) The change of the DI calculated from snapshots along with the D_{NBB}.

The appearance of the threshold value of D_{NBB}, above which DI drastically increases, mainly originates from the contribution of the non-linear Hamaker potential (a more intense attractive interaction between the inorganic NBBs) and also the depletion interaction.[20] The increase of D_{NBB} results in a rapid aggregation of NBBs, which collapses the ordered structure formed by the amphiphilic surfactants. This model is in excellent agreement with the observed experimental trends and illustrates not only the key role of D_{NBB} in flexible adaptation of NBBs to the micelle structure but also, more importantly, the critical role of D_{NBB} in colloidal and depletion forces which put self-assembly process into the action.

The effect of aggregation of NBB on the formation of mesoporous structures

As well as the value of D_{NBB}, the aggregative tendency of NBBs upon drying in the EISA process is another important parameter. In a previous work on mesoporous titania, simulations permitted to explain the deleterious role of aggregation between the NBBs on the order of the mesoporous structures. Namely, strong NBB-NBB attraction results in aggregation, which in turn leads to a merging of the mesopores, thus leading to poorly defined mesostructures.[20] In order to test the generality of this hypothesis, samples with higher aggregation tendency than the previously presented AA-*y*-*t* were employed to investigate this point. When acetic acid was used (AcOH-2.0-*t*) instead of acrylic acid, the aggregation tendency was higher than that in the acrylic acid system (AA-2.0-*t*) (Figure S7). Residual Ni^{2+} ions, D_p, and zeta potentials of particles were comparable between both systems at a given reaction time (Table 1). However, the AcOH-containing colloids present a higher degree of aggregation, that results formation of a larger aggregate. This difference in the aggregation behavior suggests a different interparticle interaction, originated from different London-van der Waals forces derived from both surface modifiers. This points out that attention has to be paid to the intimate structure and interactions in the NBB (i.e., using AA and AcOH as reaction controllers).

Figure 6 shows the SAXS patterns of films prepared from F-AcOH-2.0-*t* solutions. The resultant mesostructures were assigned to the same cubic mesostructures (space group; *Im–3m*) as F-AA-*y*-*t* systems. However, the threshold of D_{NBB} = 1.3 nm for the formation of ordered mesostructures is significantly smaller compared with the F-AA-*y*-*t* systems (D_{NBB} < 7.5 nm). It is interesting to remark that albeit the AcOH-derived NBB are small and in principle should lead to high organization, they tend to aggregate (as discussed above), which increases the effective size of the building blocks and changes the effective interactions with the template. D_S of the F-AcOH-2.0 systems begins to increase significantly after 20 minutes aging with respect to the equivalent AA-derived samples. In the case of F-AcOH-2.0-*60*, for example, D_S = 7.9nm, which is in fact practically twice the critical NBB size found in the theoretical model for obtaining ordered mesostructures. This demonstrates that the aggregation tendency is an essential parameter to synthesize highly organized mesostructures, which should be taken care of, as well as controlling the D_{NBB} below a certain critical size.

Table 1. The comparison of AA-2.0-t and AcOH-2.0-t systems.

ID	Residual Ni^{2+} (%)	D_p / nm	D_s / nm	Zeta potential / mV (pH)
AA-2.0-5	33.0	0.74	N/A	29.6 (8.0)
AA-2.0-60	4.4	2.1	N/A	32.2 (8.2)
AcOH-2.0-5	33.7	0.99	N/A	28.6 (6.2)
AcOH-2.0-60	3.9	2.0	7.9	32.9 (8.3)

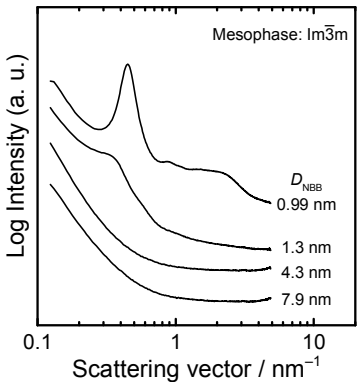

Figure 6. SAXS patterns of casted-films after drying at 120 °C for 2h. The casted-films composed of D_{NBB} = 0.99 nm, 1.3 nm, 4.3 nm, and 7.9 nm were prepared from F-AcOH-2.0-5, F-AcOH-2.0-10, F-AcOH-2.0-30, and F-AcOH-2.0-60, respectively. D_{NBB} of 4.3 nm and 7.9 nm are D_s and their D_p are 1.7 nm and 2.0 nm, respectively.

Extending the ANBB Approach to Other Transition Metal Hydroxides.

The ANBB approach presented above was extended to hydroxide NBBs for a series of divalent elements (Mn, Fe, Co, and Cu), based on the insights obtained in the α-Ni(OH)$_2$ NBB system. Controlling the crystallization in the respective systems was allowed through the choice of carboxylic acids (Figure S8 and Table S1). According to the literature,[30] metal hydroxo clusters can be formed through M-OH-M bond formation upon leaving of the aqua-ligand. Therefore, the rate of the formation of NBBs strongly depends on a lability of the ligand. It was found that NBBs were controllably grown by using a carboxylic acid with an appropriate coordination strength. A polyprotic carboxylic acid with stronger coordination characteristic can be used for a divalent metal element with more labile aqua-ligand. By this way, a general and versatile synthesis of the metal hydroxo NBB and their assembly into mesostructured films can be achieved by simply optimizing the kinetics of crystal growth and aggregation (Figure 7). High ordering is allowed by the appropriate choice and combination of the metal ion and an adequate carboxylic acid.

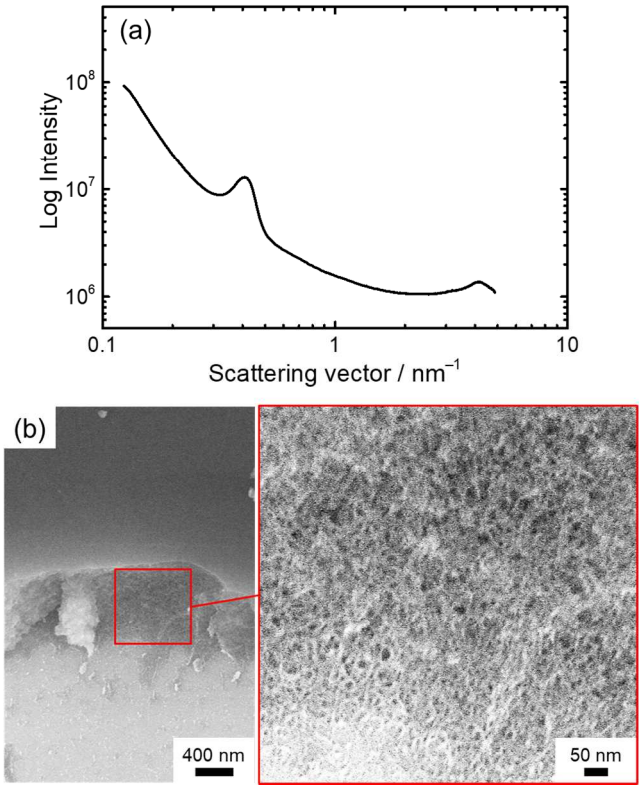

Figure 7. SAXS patterns of cast-film of Co-Cit-0.67-0.5 after drying at 120 °C for 2h. (b) Cross sectional SEM images of Co-Cit-0.67-0.5 after heat treatment at 120 °C for 2 h and 250 °C for 2 h.

Conclusion

In this work, we report the controlled synthesis of colloidal α-Ni(OH)$_2$ NBBs with a variety of diameters in the nanometer scale -from oligomer to over 20 nm- by controlling the crystallization and aggregation kinetics via a homogeneous epoxide-mediated alkalinization process. Highly ordered mesostructures were obtained when the α-Ni(OH)$_2$ NBBs with a size less than a critical value were employed in combination with F127 templates. A computational model in conjunction with simulations showed an excellent agreement with experimental results and predictive power, which is useful for the actual design of the synthetic pathway. This analysis reveals that the D_{NBB} is a critical parameter to obtain the ordered mesoporous structures. It was also found that the aggregation tendency (stability of NBBs) significantly affects the thresholds of D_{NBB} toward ordered mesostructures; the NBBs with lower aggregation tendency showed a wider D_{NBB} range for ordered mesostructure formation. To prepare NBBs and mesostructured films for a variety of chemical compositions, an appropriate combination of a metal and a carboxylic acid in each system is mandatory for the inhibition of crystal growth and retarding aggregation. The approach demonstrated here is a promising general route to access versatile functional mesoporous and mesostructured materials, in particular those based on low-valence transition metal oxides. In addition, as this method is

based on EISA, a flexible processing can lead towards thin films, xerogels or aerosols.

We anticipate that this pathway that employs pre-defined, controlled and stable inorganic NBBs will permit to circumvent the chemical complexities of solution processing. In addition, the feedback between experiments and theory permits to consider a "chemistry of objects", in which the co-self-assembly of pre-programmed soft and colloidal objects can be envisioned. Following a simple set of rules, based on controlling the size of different NBB, their interactions and aggregation behavior, complex architectures can be created by simple combination of building blocks "from the shelf".

ASSOCIATED CONTENT

Supporting Information. FT-IR spectra, UV-Vis-NIR spectra, PXRD patterns, SAXS patterns, simulated snapshots, N_2 sorption/desorption, TEM image. This material is available free of charge via the Internet at http://pubs.acs.org.

AUTHOR INFORMATION

Corresponding Author

* E-mail (Y. Tokudome): tokudome@photomater.com
* E-mail (G. J. A. A. Soler-Illia): gsoler-illia@unsam.edu.ar
Present address of NT: Department of Chemical Science and Technology, Faculty of Bioscience and Applied Chemistry, Hosei University, Koganei, Tokyo 184-8584, Japan

ACKNOWLEDGMENT

Strategic Young Researcher Overseas Visits Program for Accelerating Brain Circulation from JSPS is gratefully acknowledged. The present work was partially supported by JSPS KAKENHI, JSPS bilateral program, ABTLuS (LNLS proposal SAXS1 18927), ANPCyT (PICT 2014-3687 and 2015-3526), UBACyT (20020130100610BA), The Sumitomo Foundation, Izumi Science and Technology Foundation and Deutsche Forschungsgemeinschaft-CONICET under grant Mu1674/15-1. The simulations have been performed at the GWDG Göttingen, the HLRN Hannover/Berlin, and the von-Neumann Institute for Computing, Jülich, Germany.

REFERENCES

(1) Guo, J.; Tardy, B.; Christofferson, A.; Dai, Y.; Richardson, J.; Zhu, W.; Hu, M.; Ju, Y.; Cui, J.; Dagastine, R.; Yarovsky, I.; Caruso, F. Modular Assembly of Superstructures from Polyphenol-Functionalized Building Blocks. *Nat. Nanotechnol.* **2016**, *11*, 1105–1111.

(2) Armao, J.; Nyrkova, I.; Fuks, G.; Osypenko, A.; Maaloum, M.; Moulin, E.; Arenal, R.; Gavat, O.; Semenov, A.; Giuseppone, N. Anisotropic Self-Assembly of Supramolecular Polymers and Plasmonic Nanoparticles at the Liquid-Liquid Interface. *J. Am. Chem. Soc.* **2017**, *139*, 2345-2350.

(3) Wang, Y.; Price, A.; Caruso, F. Nanoporous Colloids: Building Blocks for a New Generation of Structured Materials. *J. Mater. Chem.* **2009**, *19*, 6451–6464.

(4) Ding, H.; Liu, C.; Gu, H.; Zhao, Y.; Wang, B.; Gu, Z. Responsive Colloidal Crystal for Spectrometer Grating. *ACS Photonics* **2014**, *1*, 121–126.

(5) Tokudome, Y.; Nakanishi, K.; Kanamori, K.; Fujita, K.; Akamatsu, H.; Hanada, T. Structural Characterization of Hierarchically Porous Alumina Aerogel and Xerogel Monoliths. *J. Colloid Interface Sci.* **2009**, *338*, 506–513.

(6) Yamada, Y.; Tsung, C.-K.; Huang, W.; Huo, Z.; Habas, S.; Soejima, T.; Aliaga, C.; Somorjai, G.; Yang, P. Nanocrystal Bilayer for Tandem Catalysis. *Nat. Chem.* **2011**, *3*, 372–376.

(7) Wang, Y.; Jenkins, I.; McGinley, J.; Sinno, T.; Crocker, J. Colloidal Crystals with Diamond Symmetry at Optical Lengthscales. *Nat. Commun.* **2017**, *8*, 14173.

(8) Xiao, X.; Yu, H.; Jin, H.; Wu, M.; Fang, Y.; Sun, J.; Hu, Z.; Li, T.; Wu, J.; Huang, L.; Gogotsi, Y.; Zhou, J. Salt-Templated Synthesis of 2D Metallic MoN and Other Nitrides. *ACS Nano* **2017**, *11*, 2180-2186.

(9) Li, B. W.; Osada, M.; Ozawa, T. C.; Ebina, Y.; Akatsuka, K.; Ma, R.; Funakubo, H.; Sasaki, T., Engineered Interfaces of Artificial Perovskite Oxide Superlattices via Nanosheet Deposition Process. *ACS Nano* **2010**, *4*, 6673–6680.

(10) Wang, L.; Wang, D.; Dong, X. Y.; Zhang, Z. J.; Pei, X. F.; Chen, X. J.; Chena , B.; Jin, J. Layered assembly of graphene oxide and Co–Al layered double hydroxide nanosheets as electrode materials for supercapacitors. *Chem. Commun.* **2011**, *47*, 3556–3558.

(11) Sanchez, C.; Boissière, C.; Grosso, D.; Laberty, C.; Nicole, L. Design, Synthesis, and Properties of Inorganic and Hybrid Thin Films Having Periodically Organized Nanoporosity. *Chem. Mater.* **2008**, *20*, 682–737.

(12) Wong, M.; Jeng, E.; Ying, J. Supramolecular Templating of Thermally Stable Crystalline Mesoporous Metal Oxides Using Nanoparticulate Precursors. *Nano Lett.* **2001**, *1*, 637–642.

(13) Hwang, Y.; Lee, K.-C.; Kwon, Y.-U. Nanoparticle Routes to Mesoporous Titania Thin Films. *Chem. Commun.* **2001**, 738–1739.

(14) Chane-Ching, J.; Cobo, F.; Aubert, D.; Harvey, H.; Airiau, M.; Corma, A. A General Method for the Synthesis of Nanostructured Large-Surface-Area Materials through the Self-Assembly of Functionalized Nanoparticles. *Chem. - Eur. J.* **2005**, *11*, 979–987.

(15) Fan, K.; Chen, H.; Ji, Y.; Huang, H.; Claesson, P.; Daniel, Q.; Philippe, B.; Rensmo, H.; Li, F.; Luo, Y.; Sun, L. Nickel-Vanadium Monolayer Double Hydroxide for Efficient Electrochemical Water Oxidation. *Nat. Commun.* **2016**, 7, 11981.

(16) Nguyen, T.; Boudard, M.; Carmezim, J.; Montemor, F. $Ni_xCo_{1-x}(OH)_2$ Nanosheets on Carbon Nanofoam Paper as High Areal Capacity Electrodes for Hybrid Supercapacitors. *Energy* **2017**, *126*, 208–216.

(17) Lee, A. F.; Bennett, J. A.; Manayil, J. C.; Wilson, K. Heterogeneous catalysis for sustainable biodiesel production via esterification and transesterification. *Chem. Soc. Rev.* **2014**, *43*, 7887–7916.

(18) Yu, X.-Y.; Luo, T.; Jia, Y.; Xu, R.-X.; Gao, C.; Zhang, Y.-X.; Liu, J.-H.; Huang, X.-J. Three-Dimensional Hierarchical Flower-like Mg–Al-Layered Double Hydroxides: Highly Efficient Adsorbents for As(v) and Cr(vi) Removal. *Nanoscale* **2012**, *4*, 3466–3474.

(19) Tarutani, N.; Tokudome, Y.; Jobbágy, M.; Viva, F.; Soler-Illia, G.; Takahashi, M. Single-Nanometer-Sized Low-Valence Metal Hydroxide Crystals: Synthesis via Epoxide-Mediated Alkalinization and Assembly toward Functional Mesoporous Materials. *Chem. Mater.* **2016**, *28*, 5606–5610.

(20) Tang, Q.; Angelomé, P. C.; Soler-Illia, G. J. A. A.; Müller, M. Formation of Ordered Mesostructured TiO_2 Thin Films: A Soft Coarse-Grained Simulation Study. *Phys. Chem. Chem. Phys.* **2017**, *19*, 28249–28262.

(21) Gash, A.; Tillotson, T.; Satcher, J.; Poco, J.; Hrubesh, L.; Simpson, R. Use of Epoxides in the Sol–Gel Synthesis of Porous Iron(III) Oxide Monoliths from Fe(III) Salts. *Chem. Mater.* **2001**, *13*, 999–1007.

(22) Tokudome, Y.; Tarutani, N.; Nakanishi, K.; Takahashi, M. Layered Double Hydroxide (LDH)-Based Monolith with Interconnected Hierarchical Channels: Enhanced Sorption Affinity for Anionic Species. *J. Mater. Chem. A* **2013**, *1*, 7702–7708.

(23) Soler-Illia, G. J. A. A.; Jobbágy, M.; Regazzoni, A. E.; Blesa, M. Synthesis of Nickel Hydroxide by Homogeneous Alkalinization. Precipitation Mechanism. *Chem. Mater.* **1999**, *11*, 3140-3146.

(24) Manceau, A.; Calas, G; Decarreau, A. Nickel-Bearing Clay Minerals: I. Optical Spectroscopic Study of Nickel Crystal Chemistry. *Clay Miner.* **1985**, *20*, 367–387.

(25) Poul, L.; Jouini, N.; Fiévet, F. Layered Hydroxide Metal Acetates (Metal = Zinc, Cobalt, and Nickel): Elaboration via Hydrolysis in Polyol Medium and Comparative Study. *Chem. Mater.* **2000**, *12*, 3123-3132.

(26) Deacon, G.B.; Phillips R.J. Relationships Between the Carbon-Oxygen Stretching Frequencies of Carboxylato Complexes and the Type of Carboxylate Coordination. *Coord. Chem. Rev.* **1980**, *33*, 227-250.

(27) Lopez, L.; Benjauthrit, K.; Schelhas, L.; Stefik, M.; Augustyn, V.; Ko, J.; Dunn, B.; Wiesner, U.; Milliron, D.; Tolbert, S. General Method for the Synthesis of Hierarchical Nanocrystal-Based Mesoporous Materials. *ACS Nano* **2012**, *6*, 6386–6399.

(28) Hamaker, H.C. The London—van der Waals Attraction Between Spherical Particles. *Physica* **1937**, *4*, 1058–1072.

(29) Müller, M. Studying Amphiphilic Self-assembly with Soft Coarse-Grained Models. *J. Stat. Phys.* **2011**, *145*, 967–1016.

(30) Soler-Illia, G. J. A. A.; Louis, A.; Sanchez, C. Synthesis and Characterization of Mesostructured Titania-Based Materials through Evaporation-Induced Self-Assembly. *Chem. Mater.* **2002**, *14*, 750–759.

(31) Livage, J.; Henry, M.; Sanchez, C. Sol-Gel Chemistry of Transition Metal Oxides. *Progress in Solid State Chemistry* **1988**, *18*, 259–341.

TOC Image

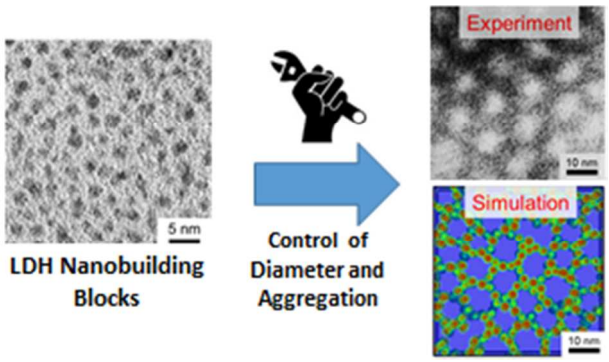
5 nm
LDH Nanobuilding Blocks
Control of Diameter and Aggregation
Experiment
10 nm
Simulation
10 nm